

# Fast and accurate 3D PSF computation for fluorescence microscopy

JIZHOU LI<sup>1,\*</sup>, FENG XUE<sup>2</sup>, AND THIERRY BLU<sup>1</sup>

<sup>1</sup>Department of Electronic Engineering, The Chinese University of Hong Kong, Shatin, N.T., Hong Kong

<sup>2</sup>National Key Laboratory of Science and Technology on Test Physics and Numerical Mathematics, Beijing, China

\*Corresponding author: jzli@ee.cuhk.edu.hk

Compiled May 8, 2017

The point-spread function (PSF) plays a fundamental role in fluorescence microscopy. A realistic and accurately calculated PSF model can significantly improve the performance in 3D deconvolution microscopy and also the localization accuracy in single-molecule microscopy. In this work, we propose a fast and accurate approximation of the Gibson-Lanni model, which has been shown to represent the PSF suitably under a variety of imaging conditions. We express the Kirchhoff's integral in this model as a linear combination of rescaled Bessel functions, thus providing an integral-free way for the calculation. The explicit approximation error in terms of parameters is given numerically. Experiments demonstrate that the proposed approach results in a significantly smaller computational time compared with current state-of-the-art techniques to achieve the same accuracy. This approach can also be extended to other microscopy PSF models. © 2017 Optical Society of America

*OCIS codes:* (180.2520) Fluorescence microscopy; (180.6900) Three-dimensional microscopy.

<http://dx.doi.org/10.1364/josaa.XX.XXXXXX>

## 1. INTRODUCTION

Fluorescence microscopy is widely used in biological research to analyze 3D structures of living cells and tissues. The point-spread function (PSF) of a microscope describes the response of this imaging system to a point source or object. An accurate PSF is highly desirable in deconvolution microscopy because of its critical influence on the restoration quality. Several works have focused on using more accurate PSF models in wide-field microscopy [1–3] or confocal microscopy [4, 5] in order to improve the resolution of the images. We focus on the 3D wide field fluorescence microscopy which is the general setting of a live cell imaging. In this case, the PSF is axially asymmetric and depth variant. The asymmetry results from the mismatch between the refractive indices of the immersion medium and of the specimen. The depth-dependence results from optical path difference between the ideal and real conditions, which depends on the depth of the object location [6].

In addition, the PSF model has also a major influence on single molecule localization microscopy [7–10]. Despite the widespread approximation of the PSF by a Gaussian, it has been argued that a more realistic model can significantly improve the localization accuracy [9, 11–13]. While a 2D PSF can be reasonably well approximated by a Gaussian kernel, no Gaussian can accurately represent a complete 3D PSF in fluorescence microscopy [14]. Indeed, the Gaussian model provides a good

approximation to the 3D PSF only within a limited spatial range near the focus. The trade-off between using simple Gaussian and realistic models is computational complexity versus accuracy.

Methods to estimate the realistic PSF can be classified into two categories, namely experimental and analytical. The experimental PSF reflects the imaging conditions and thus contains both the intrinsic and extrinsic aberrations [1]. Some works [15, 16] are trying to retrieve PSFs at various depths from a large number of measured PSFs using a method described by Hanser et al. [17]. This approach, however, has difficulties to image sub-resolution beads with low signal-to-noise ratio, thus needs to average several measurements. Moreover, the imaging conditions of experimental PSFs are different from those in actual imaging. The alternative would be to use an analytical model of the PSF, that takes into account the physical aberrations of the acquisition system.

The literature on PSF modeling in wide field microscopy is extensive, but the most popular one is the Gibson-Lanni model [6]. This model is based on the Kirchhoff's diffraction integral and a calculation of the optical path difference (OPD) between design and experimental conditions. It accounts for coverslips and other interfaces between the specimen and the objective. Compared to vectorial-based models [18, 19], the Gibson-Lanni model is simpler and has the advantage of depending only on the standard parameters of the objective and the optical properties of the specimen. It has been shown to be very useful

for deconvolution microscopy [2, 20–23] and also for particle localization [8, 12, 24, 25].

The main limitation of the Gibson-Lanni PSF model, however, is computational. Accurate computation of the Kirchoff's integral for all 3D pixels is CPU intensive. Apart from applications in single molecule localization microscopy, a fast PSF computation is necessary in 3D deconvolution microscopy. Most of the high performance deconvolution algorithms rely on repeated estimation of the PSF model [2, 26–29]. In the case of depth dependent deconvolution [2, 30, 31], multiple PSFs varying as a function of depth have to be used. After pre-computing the model PSFs at various depths, Arigovindan *et al.* [31] proposed an efficient method based on principal component analysis for the depth-varying representations. Hence, an improved model PSF calculation method is likely to result in a significant improvement in the deconvolution process. Current state-of-the-art techniques [12, 32] adopt a so-called progressive manner with the Simpson rule to calculate the integral. However, achieving adequate accuracy is still time-consuming.

In this work, we propose a fast and accurate approximation to the Gibson-Lanni PSF model by expressing the integral as a linear combination of rescaled Bessel functions. This approach is significantly more efficient computationally than current state-of-the-art techniques. In addition, using this Bessel series approximation amounts to replacing most of physical parameters by mathematical parameters. This may provide new insight into the automatic estimation or fitting of the PSF directly from the measurements.

The paper is organized as follows. In Section 2, we describe the Gibson-Lanni model and our computational approach based on the Bessel function. The discussions of the approximation error and computation time are also given. We then present our experimental results in Section 3 and conclude with a summary in Section 4.

## 2. 3D PSF COMPUTATION IN FLUORESCENCE MICROSCOPY

### A. The Gibson-Lanni model

A particular challenge in the PSF modeling of a microscope is the lack of detailed information about the exact design condition of the objective lenses. The parameters that are usually known include the optical characteristics of the objective (for example the numerical aperture) and the experimental conditions (i.e. refractive indices of the specimen and of the immersion medium, working distance etc). Thus it is desirable to obtain a general formulation of the PSF that is based on these known parameters. PSF modeling has been addressed diversely in the literature. Vectorial approaches that relay on Maxwell's equations directly, such as the Richards-Wolf model [18], the Török-Varga model [19] and Hell *et al.* [33], provide a rigorous treatment of diffraction in microscopes. On the other hand, scalar approaches use the diffraction theory of light [6, 34]. The most popular model is Gibson-Lanni's [6]. One of its advantages is that it can predict the non-symmetric patterns in the axial direction, which is due to refractive index mismatch among different layers. In contrast to vectorial models which require the evaluation of three integrals per point, scalar models involve only one integral per point and thus, are computationally less expensive. Haerberlé [35] showed that the vectorial model can also be combined with the ease of use of the Gibson-Lanni scalar approach, which has the advantage of introducing explicitly the known or sample-dependent parameters [32].

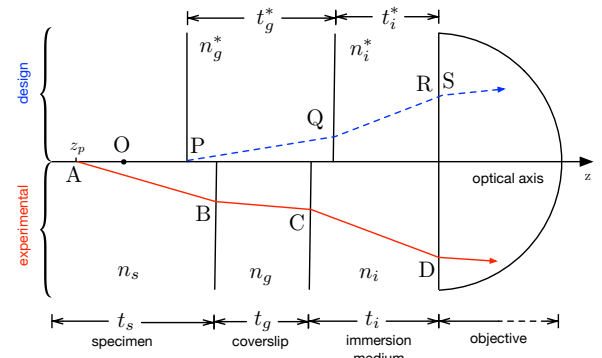


**Fig. 1.** Optical paths in the Gibson-Lanni model in the design condition (dashed line) and in the experimental condition (solid line). The optical path difference is given by  $OPD = [ABCD] - [PQRS]$ .  $\mathbf{n} = (n_i, n_i^*, n_g, n_g^*, n_s)$  and  $\mathbf{t} = (t_i, t_i^*, t_g, t_g^*, t_s)$  represent the refractive indices and the thickness values of individual layers respectively.  $z_p$  is the axial location of the point-source in the specimen relative to the cover slip.  $O$  is the origin of the coordinate system. See [6] for details.

The Gibson-Lanni model relies on the assumption that all observed aberrations are generated by factors external to the objective, and thus originate in the combination of three layers (specimen, coverslip and immersion medium). These aberrations can be characterized by the optical path difference (OPD) between a ray in a design system and one in the experimental condition, as illustrated in Fig. 1. The OPD is given by  $OPD = [ABCD] - [PQRS]$ , where  $[ABCD]$  is the path of a ray from a point source in a nondesign system when the object lies at a depth  $z_p$  and  $[PQRS]$  is the corresponding ray in the design system, where the point-source object is located immediately below the coverslip. See Fig. 1 and [6] for details.

Taking account into the law of refraction, the OPD is [6]:

$$OPD(\rho, z; z_p, \mathbf{p}) = (z + t_i^*) \sqrt{n_i^2 - (NA\rho)^2} + z_p \sqrt{n_s^2 - (NA\rho)^2} - t_i^* \sqrt{(n_i^*)^2 - (NA\rho)^2} + t_g \sqrt{n_g^2 - (NA\rho)^2} - t_g^* \sqrt{(n_g^*)^2 - (NA\rho)^2}, \quad (1)$$

where  $\rho$  is the normalized radius in the focal plane,  $z$  is the axial coordinate of the focal plane,  $z_p$  is the axial location of the point-source in the specimen layer relative to the cover slip and  $\mathbf{p} = (NA, \mathbf{n}, \mathbf{t})$  is a parameter vector containing the physical parameters of the optical system: NA is the numerical aperture,  $\mathbf{n} = (n_i, n_i^*, n_g, n_g^*, n_s)$  represents the refractive indices and  $\mathbf{t} = (t_i, t_i^*, t_g, t_g^*, t_s)$  is the thickness values of individual layers.

Because of the hypothesis of spatial invariance in planes perpendicular to the optical axis, the PSF is radially symmetric and then the Gibson-Lanni model can be expressed as a function of the coordinates  $r = \sqrt{(x - x_p)^2 + (y - y_p)^2}$  and  $z$ , given by [6]

$$PSF(r, z; z_p, \mathbf{p}) = \left| A \int_0^1 \exp(iW(\rho, z; z_p, \mathbf{p})) J_0(krNA\rho) \rho d\rho \right|^2,$$

where the phase term  $W(\rho, z; z_p, \mathbf{p}) = kOPD(\rho, z; z_p, \mathbf{p})$ ,  $k = 2\pi/\lambda$  is the wave number of the emitted light.  $A$  is a constant complex amplitude, and  $J_0$  denotes the Bessel function of the

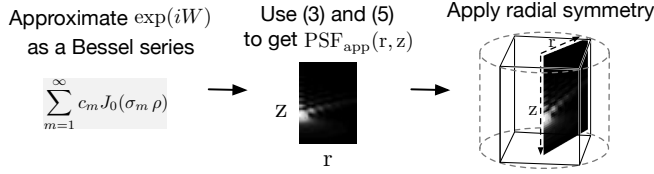


**Fig. 2.** The flow chart of the proposed PSF calculation. The inset cube is the obtained PSF.

first kind of order zero. Note that when imaging a source located at the interface ( $z_p = 0$ ), the PSF corresponds to the standard defocus model [34].

In practice, in order to ensure the validity of OPD (1), the integration intervals may not always be  $\rho \in [0, 1]$ . We set  $a = \min\{\text{NA}, n_s, n_i, n_i^*, n_g, n_g^*\} / \text{NA}$ , then the Gibson-Lanni model becomes

$$\text{PSF}(r, z; z_p, \mathbf{p}) = \left| A \int_0^a \exp(iW(\rho, z; z_p, \mathbf{p})) J_0(kr\text{NA}\rho) \rho d\rho \right|^2. \quad (2)$$

### B. Bessel series approximation

The accurate computation of the Gibson-Lanni model, however, is very time consuming because the integration in the formula (2) requires intensive numerical evaluation. This may limit applications in blind deconvolution [2, 4], PSF fitting [12] and localization microscopy [9, 24, 25].

We propose a Bessel series approximation for the Gibson-Lanni model. It is integration-free, and provides a fast and accurate approximation. The main idea is based on the fact that the integral  $\int_0^a t J_0(ut) J_0(vt) dt$  can be explicitly computed as [36]

$$\int_0^a t J_0(ut) J_0(vt) dt = a \left( \frac{u J_1(ua) J_0(va) - v J_0(ua) J_1(va)}{u^2 - v^2} \right), \quad (3)$$

when  $u \neq v$ , and  $\int_0^a t J_0(ut) J_0(vt) dt = \frac{a^2}{2} [J_1(ua)]^2$ , if  $u = v$ .

We expand the function  $\exp(iW(\rho, z; z_p, \mathbf{p}))$  in Eq. (2) as a linear combination of rescaled Bessel functions:

$$\exp(iW(\rho, z; z_p, \mathbf{p})) = \sum_{m=1}^{\infty} c_m(z) J_0(\sigma_m \rho), \quad (4)$$

where  $c_m(z)$  are complex valued coefficients (to be determined) with respect to the depth  $z$  and  $\sigma_m$  are (known) scaling factors. The usual values for the wavelength  $\lambda$  in a conventional microscope are between 340 nm and 750 nm, and the numerical aperture is often less than 1.4 [37]. In this work, we empirically set the scaling factor as  $\sigma_m = \text{NA}(3m - 2)\lambda_0 / \lambda$ , where  $\lambda_0 = 436$  nm. This series can be truncated and PSF( $r, z; z_p, \mathbf{p}$ ) is approximated using the first  $M$  terms. Then the Gibson-Lanni model in Eq. (2) is approximated by:

$$\text{PSF}_{\text{app}}(r, z; z_p, \mathbf{p}) \cong \left| A \sum_{m=1}^M c_m(z) R_m(r; \mathbf{p}) \right|^2, \quad (5)$$

where  $m = 1, 2, \dots, M, \beta = kr\text{NA}$  and

$$R_m(r; \mathbf{p}) = \frac{\sigma_m J_1(\sigma_m a) J_0(\beta a) a - \beta J_0(\sigma_m a) J_1(\beta a) a}{\sigma_m^2 - \beta^2}.$$

Through the approximation (5), the Gibson-Lanni model is now described by two physical parameters ( $\lambda$  and NA), and a set of mathematical parameters  $c_m(z)$ . Importantly, the term  $R_m(r; \mathbf{p})$

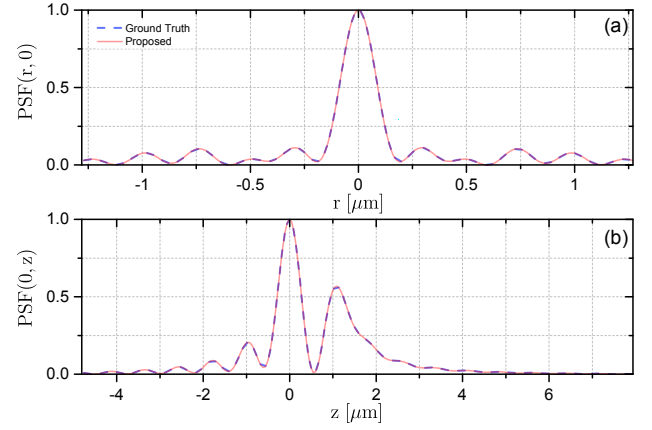


**Fig. 3.** Radial (a) and axial (b) intensity profiles (normalized) of the calculated PSF and the ground truth, for a 1.4 NA oil immersion objective, wavelength  $\lambda = 610$  nm. The point-source is located at  $z_p = 400$  nm. The ground truth is generated by the Simpson rule (the number of subintervals is set to  $10^7$ ). The number of basis functions and the sampling number in the proposed approach is set to be  $M = 10^2$  and  $K = 10^3$  respectively. The maximum difference between them is  $2.81 \times 10^{-4}$ .

needs to be calculated only once and can then be used for all slices of the 3D PSF (or any planes of same dimensions). Because of the rotational symmetry of the PSF in each slice, we compute a two times oversampled component only in one radial direction. Then, this component is resampled to a Cartesian grid using piecewise-linear interpolation. The flow chart of the proposed approach is shown in Fig. 2.

For the sake of simplicity, we omit the depth parameter  $z$  in the following representations of the coefficients  $c_m(z)$ . We use least-square fitting to determine their values. Specifically, we sample  $K$  points of  $\rho$  uniformly in the interval  $[0, a]$  as  $\rho_k = \frac{k}{K-1}a, k = 0, \dots, K-1$ , and then these coefficients can be obtained by solving the minimization problem:

$$\hat{c} = \min_c \|F - Jc\|^2,$$

where  $c = [c_1, c_2, \dots, c_M]^T$ ,  $J = [J_0(\sigma_m \rho_k)]_{1 \leq k \leq K; 1 \leq m \leq M}$ ,  $F = [f(\rho_1), f(\rho_2), \dots, f(\rho_K)]^T$ , and  $f(\rho) = \exp(iW(\rho, z; z_p, \mathbf{p}))$ . The corresponding solution is then

$$\hat{c} = (J^T J)^{-1} J^T F.$$

The approximation accuracy is controlled by the number of basis functions  $M$  and the sampling number  $K$ . Basically, larger  $M$  and  $K$  improve the approximation accuracy but with increased time cost. This will be discussed in the Section C. Fig. 3 shows a typical example of the calculated PSF where  $M = 10^2$  and  $K = 10^3$ , compared with the ground-truth PSF. Note that the non-symmetric pattern in the axis direction originates from a refractive index mismatch among different layers. It also depends on the defocus position  $z_p$ . Aguet et al. [8] studied this aberration effect in the sub-resolution axial localization and found that taking out-of-focus acquisitions can lead to a better precision in the estimation.

The computational cost of the proposed approach is mainly due to the following three aspects: 1) calculation of the basis function  $R_m(r; \mathbf{p})$  in Eq. (5); 2) determination of the coefficients  $c_m$  for each depth  $z$ ; and 3) the polar-to-Cartesian transformation

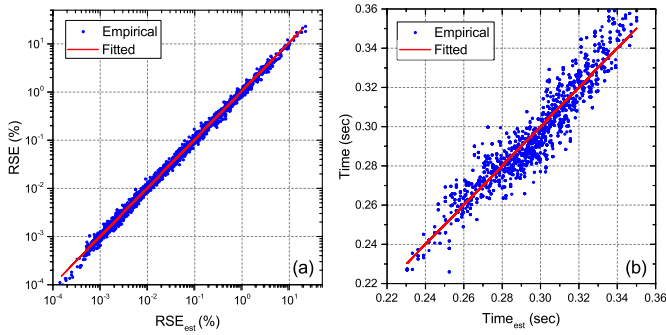


**Fig. 4.** Scatterplot demonstrating the accuracy of Eq. (6) and Eq. (7) regarding the approximation error (a) and the computational time (b). Each point corresponds to one PSF, generated by varying the design parameters  $\mathbf{p} = (\text{NA}, n, t)$ , and the approximation parameters  $K$  and  $M$ . See text for details.

from 2D components to the final 3D PSF. Typically, if the  $xyz$  dimensions of the PSF are each proportional to  $S$ , the computation cost of the first two aspects grows like  $S^2$  and  $S$ , respectively, while the cost of the interpolation step is proportional to  $S^3$ . For small PSF sizes, the time cost of the first two aspects is significant: e.g., they account for up to 47% of the total computation cost of a PSF of size  $128 \times 128 \times 64$  (when  $M = 10^2$  and  $K = 10^3$ ). For large sizes though, the total computation cost is essentially dominated by the interpolation step.

### C. Analysis of error and computational time

We performed analysis on different settings: the wavelength  $\lambda$  is in the range from 340 nm to 750 nm with a step of 50 nm; the numerical aperture NA is from 1.0 to 1.4 with a step of 0.02; and the refractive index of the specimen  $n_s$  is from 1.3 to 1.5 with a step of 0.05. There are totally 10080 PSFs of size  $256 \times 256 \times 128$ . We first generate these PSFs independently based on Simpson rule. The number of subintervals is set to  $10^7$ . This procedure is very time consuming thus not practical, but useful to provide a set of ground-truth PSFs. All experiments are carried out on a iMac with a 2.7 GHz Intel Core i5, with 4 GB of RAM. The approximation error is measured by the relative squared error (RSE) [14], defined as

$$\text{RSE} := \frac{\|\text{PSF} - \text{PSF}_{\text{app}}\|_2^2}{\|\text{PSF}\|_2^2} \times 100\%,$$

where  $\text{PSF}_{\text{app}}$  is the approximated PSF and  $\text{PSF}$  is the ground truth.

Empirically, as shown in Fig. 4(a), the approximation error  $\text{RSE}(M, K)$  with respect to the number of basis functions  $M$  and the sampling number  $K$  when  $M \in [30, 100]$  and  $K \in [50, 1000]$  can be well described by

$$\text{RSE}_{\text{est}}(M, K) = \left(\frac{M}{45}\right)^{-6.5} \left(\frac{K}{80}\right)^{-1.5}. \quad (6)$$

Compared with the sampling number  $K$ , larger  $M$  leads to a faster decay rate in the approximation error. The computational time can be described as

$$\text{Time}_{\text{est}}(M, K) = 2.87 \times 10^{-4} M + 3.63 \times 10^{-5} K + 0.22, \quad (7)$$

as shown in Fig. 4(b). Different computational environments may have different expressions for  $\text{Time}_{\text{est}}$ . However, given an

approximation error  $\epsilon$ , we can solve the following minimization problem to find the optimal approximation parameters  $M$  and  $K$ :

$$\min_{M, K} \text{Time}_{\text{est}}(M, K), \text{ s.t. } \text{RSE}_{\text{est}}(M, K) = \epsilon.$$

The corresponding solution can be obtained as

$$\begin{cases} M = 43.50 \epsilon^{-1/8}, \\ K = 1.8M. \end{cases}$$

## 3. EXPERIMENTAL RESULTS

### A. Comparison with state-of-the-art techniques

As a typical example, we set the parameters of a microscope as follows:  $\text{NA} = 1.4$ ,  $\lambda = 610$  nm,  $n_s = n_s^* = 1.33$ ,  $n_i = n_i^* = 1.5$ ,  $n_g = n_g^* = 1.5$ ,  $t_i^* = 150$   $\mu\text{m}$ ,  $t_g = 170$   $\mu\text{m}$ ,  $t_g = t_g^*$ , the lateral resolution  $\Delta_{xy}$  is 100 nm, the axial resolution  $\Delta_z$  is 250 nm and the position of the point-source  $z_p = 2000$  nm.

We compare with two state-of-the-art techniques, psf-Model [32] and PSFGenerator [12] for the computation of 3D PSF in fluorescence microscopy. psfModel is available at <http://www.francoisaguet.net/software.html> and PSFGenerator is available at <http://bigwww.epfl.ch/algorithms/psfgenerator>. Note that psfModel only supports odd dimensions. To evaluate the computation time subject to the same approximation accuracy, we now choose the number of basis functions  $M$  and the sampling number  $K$  so that the resulting RSE is identical to the RSEs in the other two techniques. Fig. 5 shows the computational time comparison for different image sizes with psfModel and PSFGenerator ('Best' option) under the same approximation accuracy. It is found, in particular, that the proposed approach is roughly 64 times faster than psfModel and 498 times faster than PSFGenerator for image size  $511 \times 511 \times 255$ . It is worth mentioning that the proposed method is implemented using unoptimized MATLAB code only (no mex files), which contrasts with the C++/Java optimized code of other algorithms.

### B. Speed comparison with a Gaussian

We also compared with the computation of Gaussian function, which is commonly used in single molecule localization microscopy. Such approximation, however, discards the side-lobes of the PSF, which are particularly important in 3D PSF modelling [12, 14]. Table. 1 shows the computational time of a Gaussian function and the proposed approach with different PSF sizes. The approximation error of our approach is set to be  $\text{RSE} = 0.1\%$ . This comparison shows that the computation of a realistic PSF requires comparable computational cost as the computation of a Gaussian, facilitating its possible use in localization microscopy.

**Table 1.** Comparison of computational time (sec.) with Gaussian function. Memory management issues explain the discrepancy between the large PSF and smaller ones.

	$128 \times 128 \times 64$	$256 \times 256 \times 128$	$512 \times 512 \times 256$	$1024 \times 1024 \times 512$
Gaussian	0.015	0.130	1.011	29.627
Proposed	0.022	0.161	1.152	15.490

## 4. CONCLUSION

We have proposed a fast and accurate calculation method of the Gibson-Lanni model for estimating the 3D PSF in fluorescence

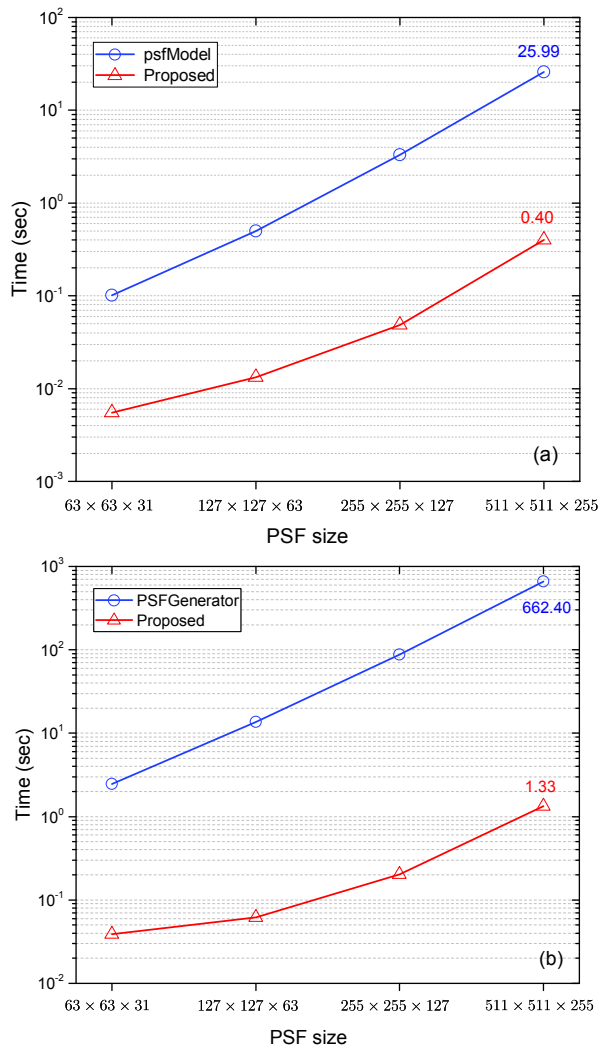


**Fig. 5.** Comparison of computational time with (a) psf-Model [32] and (b) PSFGenerator [12] for a variety of image sizes. The approximation parameters  $M$  and  $K$  in the proposed approach are chosen to result in the same accuracy RSEs as the other technique. Computational times have been averaged over 10 realizations.

microscopy. The proposed approach significantly outperforms state-of-the-art techniques. Using this new approach for estimating a realistic PSF model, is expected to improve the restoration performance in 3D deconvolution microscopy, and also the resolution in single molecule localization microscopy.

We present some preliminary results in [23] on the restoration of 3D fluorescence microscopy images using the calculated PSFs by the proposed approach. The blind estimation of the microscopy PSF and its evaluation on the restoration accuracy will be our future works. Note that it is also possible to extend the proposed approach to other scalar-based models, such as the Born-Wolf model [34], and even vector-based models, such as the Richards-Wolf model [18, 32] and the Török-Varga model [19, 35]. The source codes are available at <http://www.ee.cuhk.edu.hk/~tblu/demos>.

**Funding.** Research Grants Council (RGC) of Hong Kong (AoE/M-05/12, CUHK14200114); National Natural Science Foundation of China (NSFC) (61401013).

## REFERENCES

- J. W. Shaevitz and D. A. Fletcher, "Enhanced three-dimensional deconvolution microscopy using a measured depth-varying point-spread function," *J. Opt. Soc. Am. A* **24**, 2622–2627 (2007).
- B. Kim and T. Naemura, "Blind depth-variant deconvolution of 3D data in wide-field fluorescence microscopy," *Sci. Rep.* **5**, 9894 (2015).
- S. Ghosh and C. Preza, "Fluorescence microscopy point spread function model accounting for aberrations due to refractive index variability within a specimen," *J. Biomed. Opt.* **20**, 07500301–07500312 (2015).
- P. Pankajakshan, B. Zhang, L. Blanc-Féraud, Z. Kam, J.-C. Olivo-Marín, and J. Zerubia, "Blind deconvolution for thin-layered confocal imaging," *Appl. Opt.* **48**, 4437–4448 (2009).
- M. A. Bruce and M. J. Butte, "Real-time GPU-based 3D deconvolution," *Opt. Express* **21**, 4766–4773 (2013).
- S. F. Gibson and F. Lanni, "Experimental test of an analytical model of aberration in an oil-immersion objective lens used in three-dimensional light microscopy," *J. Opt. Soc. Am. A* **9**, 154–166 (1992).
- M. Speidel, A. Jonáš, and E.-L. Florin, "Three-dimensional tracking of fluorescent nanoparticles with subnanometer precision by use of off-focus imaging," *Opt. Lett.* **28**, 69–71 (2003).
- F. Aguet, D. Van De Ville, and M. Unser, "A maximum-likelihood formalism for sub-resolution axial localization of fluorescent nanoparticles," *Opt. Express* **13**, 10503–10522 (2005).
- D. Sage, H. Kirshner, T. Pengo, N. Stuurman, J. Min, S. Manley, and M. Unser, "Quantitative evaluation of software packages for single-molecule localization microscopy," *Nat. Methods* **12**, 717–724 (2015).
- Y. Ding and C. Li, "Dual-color multiple-particle tracking at 50-nm localization and over 100- $\mu\text{m}$  range in 3d with temporal focusing two-photon microscopy," *Biomed. Opt. Express* **7**, 4187–4197 (2016).
- S. Stallinga and B. Rieger, "Accuracy of the gaussian point spread function model in 2d localization microscopy," *Opt. Express* **18**, 24461–24476 (2010).
- H. Kirshner, F. Aguet, D. Sage, and M. Unser, "3-D PSF fitting for fluorescence microscopy: implementation and localization application," *J. Microsc.* **249**, 13–25 (2013).
- A. Small and S. Stahlheber, "Fluorophore localization algorithms for super-resolution microscopy," *Nat. Methods* **11**, 267–279 (2014).
- B. Zhang, J. Zerubia, and J.-C. Olivo-Marín, "Gaussian approximations of fluorescence microscope point-spread function models," *Appl. Opt.* **46**, 1819–1829 (2007).
- E. Maalouf, B. Colicchio, and A. Dieterlen, "Fluorescence microscopy three-dimensional depth variant point spread function interpolation using zernike moments," *J. Opt. Soc. Am. A* **28**, 1864–1870 (2011).
- S. Liu, E. B. Kromann, W. D. Krueger, J. Bewersdorf, and K. A. Lidke, "Three dimensional single molecule localization using a phase retrieved pupil function," *Opt. Express* **21**, 29462–29487 (2013).
- B. M. Hanser, M. G. L. Gustafsson, D. A. Agard, and J. W. Sedat, "Phase-retrieved pupil functions in wide-field fluorescence microscopy," *J. Microsc.* **216**, 32–48 (2004).
- B. Richards and E. Wolf, "Electromagnetic diffraction in optical systems II. structure of the image field in an aplanatic system," *P. Roy. Soc. Lond. A Mat.* **253**, 358–379 (1959).
- P. Török and P. Varga, "Electromagnetic diffraction of light focused through a stratified medium," *Appl. Opt.* **36**, 2305–2312 (1997).
- C. Preza and J.-A. Conchello, "Depth-variant maximum-likelihood restoration for three-dimensional fluorescence microscopy," *J. Opt. Soc. Am. A* **21**, 1593–1601 (2004).
- J. Kim, S. An, S. Ahn, and B. Kim, "Depth-variant deconvolution of 3d widefield fluorescence microscopy using the penalized maximum likelihood estimation method," *Opt. Express* **21**, 27668–27681 (2013).
- B. Kim and T. Naemura, "Blind deconvolution of 3D fluorescence microscopy using depth-variant asymmetric PSF," *Microsc. Res. Tech.* (2016).
- J. Li, F. Luisier, and T. Blu, "PURE-LET deconvolution of 3D fluorescence microscopy images," in "Proceedings of IEEE International Symposium on Biomedical Imaging (IEEE, 2017)," (to be published).
- T. Ilovitsh, A. Weiss, A. Meiri, C. G. Ebeling, A. Amiel, H. Katz, B. Mannasse-Green, and Z. Zalevsky, "K-factor image deshadowing

- for three-dimensional fluorescence microscopy," *Sci. Rep.* **5**, 13724 (2015).
25. J. Huang, M. Sun, K. Gumpfer, Y. Chi, and J. Ma, "3D multifocus astigmatism and compressed sensing (3D MACS) based superresolution reconstruction," *Biomed. Opt. Express* **6**, 902–917 (2015).
26. E. F. Y. Hom, F. Marchis, T. K. Lee, S. Haase, D. A. Agard, and J. W. Sedat, "AIDA: an adaptive image deconvolution algorithm with application to multi-frame and three-dimensional data," *J. Opt. Soc. Am. A* **24**, 1580–1600 (2007).
27. C. Vonesch and M. Unser, "A fast thresholded landweber algorithm for wavelet-regularized multidimensional deconvolution," *IEEE Trans. Image Process.* **17**, 539–549 (2008).
28. F. Soulez, L. Denis, Y. Tourneur, and E. Thiébaud, "Blind deconvolution of 3D data in wide field fluorescence microscopy," in "Proceedings of IEEE International Symposium on Biomedical Imaging (IEEE, 2012)," pp. 1735–1738.
29. D. Sage, L. Donati, F. Soulez, D. Fortun, G. Schmit, A. Seitz, R. Guiet, C. Vonesch, and M. Unser, "Deconvolutionlab2: An open-source software for deconvolution microscopy," *Methods* **115**, 28–41 (2017).
30. J. W. Shaevitz and D. A. Fletcher, "Enhanced three-dimensional deconvolution microscopy using a measured depth-varying point-spread function," *J. Opt. Soc. Am. A* **24**, 2622–2627 (2007).
31. M. Arigovindan, J. Shaevitz, J. McGowan, J. W. Sedat, and D. A. Agard, "A parallel product-convolution approach for representing depth varying point spread functions in 3d widefield microscopy based on principal component analysis," *Opt. Express* **18**, 6461–6476 (2010).
32. F. Aguet, "Super-resolution fluorescence microscopy based on physical models," Ph.D. thesis, Ecole Polytechnique Fédérale de Lausanne (2009).
33. S. Hell, G. Reiner, C. Cremer, and E. H. Stelzer, "Aberrations in confocal fluorescence microscopy induced by mismatches in refractive index," *Journal of microscopy* **169**, 391–405 (1993).
34. M. Born and E. Wolf, *Principles of optics: electromagnetic theory of propagation, interference and diffraction of light* (Cambridge University Press, 1999).
35. O. Haeberlé, "Focusing of light through a stratified medium: a practical approach for computing microscope point spread functions. Part I: conventional microscopy," *Opt. Commun.* **216**, 55–63 (2003).
36. G. N. Watson, *A treatise on the theory of Bessel functions* (Cambridge university press, 1995).
37. D. B. Murphy and M. W. Davidson, *Fundamentals of Light Microscopy and Electronic Imaging* (John Wiley & Sons, Inc., 2012).